SQUEEZE CRITERIA & REQUIREMENTS

Oliver Brüning, CERN, Geneva, Switzerland

Abstract

The procedure for squeezing the LHC is defined with attention to the squeeze duration, the variation in magnet currents and the resulting limitations. The potential variation in key beam parameters is quantified. The demands on essential sub-systems [feedback, instrumentation and controls] are made clear. The requisite movement of the collimators and TCDQ during the squeeze are detailed.

REQUIREMENTS DURING THE SQUEEZE

SUMMARY OF LUMINOSITY OPTICS AND CROSSING ANGLE PARAMETERS

Table 1 and 2 summarize the optics and crossing angle configurations in the experimental insertions (IR) at injection and physics optics configurations respectively. Fig. 1 and 3 show the corresponding β- and dispersion functions for Beam1 and Fig. 2 and 4 the corresponding crossing angle orbit bumps over IR1 and IR5. Fig. 4 shows the pre-collision crossing angle bump which still features a parallel separation of ± 0.5 mm at the interaction point (IP). The crossing angle orbit bumps generate a minimum beam separation of 9.0 σ and 6.9 σ along the common vacuum beam pipe in the long straight section for the injection and physics optics configurations respectively. The parallel separation at the IP is removed during physics operation. A detailed description of the crossing angle and optics configurations in all experimental insertions can be found in the LHC design report [1].

Table 1: Optics and crossing angle configuration in the four experimental insertions for the injection optics. β^* denotes the β-function at the interaction point, ϕ the half-crossing angle and Δ the half parallel separation at the IP and L the design luminosity for physics operation with proton beams.

IR	β^* **[m]**	ϕ **[mm]**	Δ $[\mu$**rad]**	L $[cm^{-2}sec^{-1}]$
IR1	18.0	$\pm$160 (V)	$\pm$2.6 (H)	0
IR2	10.0	$\pm$240 (V)	$\pm$2.0 (H)	0
IR5	18.0	$\pm$160 (H)	$\pm$2.6 (V)	0
IR8	10.0	$\pm$300 (H)	$\pm$2.0 (V)	0

The squeeze describes the transition from the injection to the physics optics configuration. The goal of the squeeze is to generate an optics transition in the experimental insertions with a minimum perturbation of the optics in the rest of the machine and maintaining a minimum beam separation of 6.9 σ along the common vacuum chamber in the long straight section. Table 3 summarizes the main optics and orbit tolerances that are compatible with the collimation system and the mechanical acceptance of the LHC [1]. Maintaining the tolerances in Table 3 requires an excellent optics control during the squeeze which in turn requires either an excellent knowledge of the magnet transfer functions and power converter control or online feedback systems. In order to facilitate the magnet transfer function model and the optics control during the squeeze the optics design aims at a smooth transition of the magnet powering during the squeeze and tries to avoid zero crossings and small gradients (which imply large persistent current effects) where possible.

Table 2: Optics and crossing angle configuration in the four experimental insertions for the physics configuration. β^* denotes the β-function at the interaction point (IP), ϕ the half-crossing angle and Δ the half parallel separation at the IP and L the design luminosity for physics operation with proton beams.

IR	β^* **[m]**	ϕ **[mm]**	Δ $[\mu$**rad]**	L $[cm^{-2}sec^{-1}]$
IR1	0.55	$\pm$142.5 (V)	$\pm$0.0 (H)	10^{34}
IR2	10.0	$\pm$150 (V)	$\pm$0.18 (H)	10^{30}
IR5	0.55	$\pm$142.5 (H)	$\pm$0.0 (V)	10^{34}
IR8	10.0 1 / 35	$\pm$75 (H)	$\pm$0.0 (V)	10^{32}

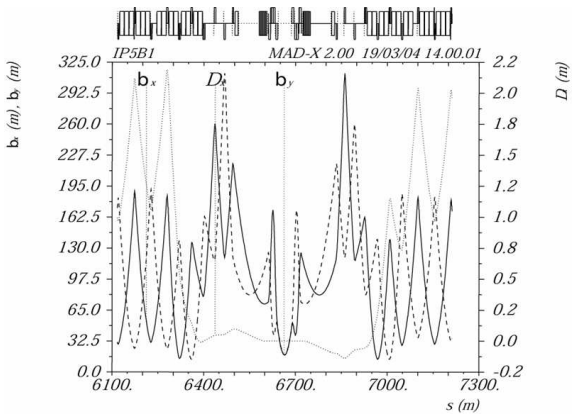

Figure 1: The injection optics in IR5 for Beam1.

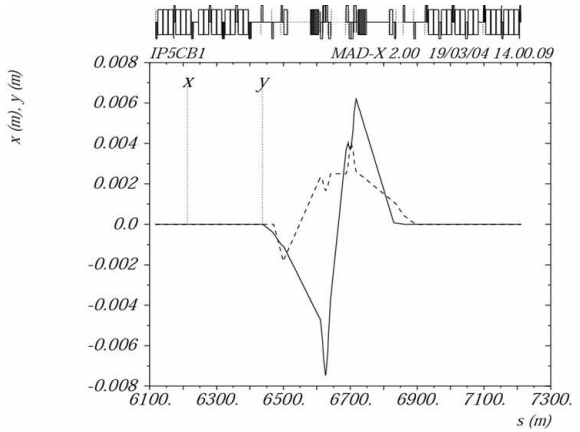

Figure 2: The crossing angle separation scheme for the injection optics configuration in IR5 for Beam1.

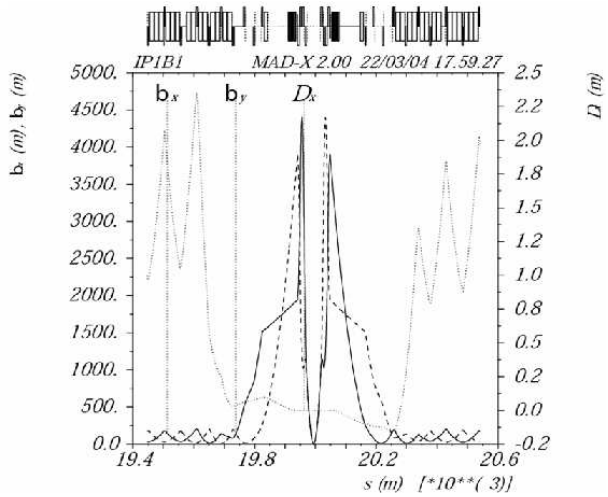

Figure 3: The collision optics in IR1 for Beam1.

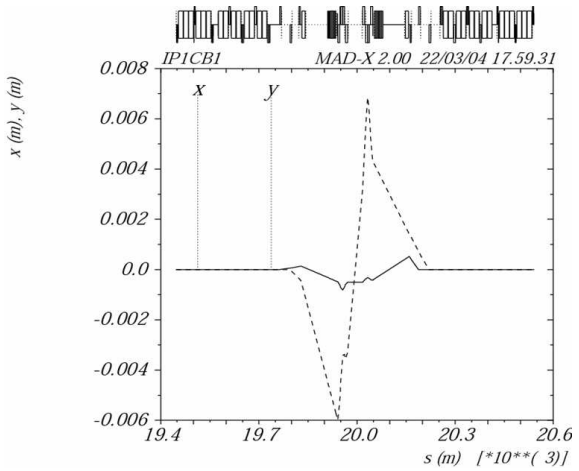

Figure 4: The crossing angle separation scheme for the pre-collision optics configuration in IR5 for Beam1.

Table 3: The main optics and orbit tolerances that are compatible with the LHC collimation system and mechanical acceptance.

Parameter	**Tolerance**
Tune change	$\Delta Q < 0.01$
β-beat	21%
Spurious dispersion	27 % of nominal normalized dispersion in arc
closed orbit in IR	± 3 mm inside triplet magnets
closed orbit in the cleaning insertions	$\pm 0.2\sigma$ of the nominal beam size
Change in beam separation	$\Delta\delta < 1\sigma$

GRADIENT TRANSITION DURING SQUEEZE

Fig. 5 to 10 show the transition optics solution in IR5 for Beam1 and Fig. 11 to 14 the corresponding gradient transitions for the individually powered insertion quadrupole magnets. Fig. 15 and 16 show the gradients for the 600 A trim quadrupole circuits in the dispersion suppressors [2]. All quadrupole magnets are powered with at least 50 % of their nominal current at the end of the ramp and persistent current effects should not play an important role at this stage. However, some quadrupole currents are considerably reduced during the squeeze. For example, the powering current in Q6 corresponds only to approximately 5 % of the nominal current at the end of the squeeze and persistent current effects became relevant again at this point. Another interesting example is the powering current of the Q5 magnets which changes from almost 100 % of the nominal powering at the end of the ramp to approximately 30 % at the end of the squeeze. This is clearly larger than the minimum powering level in the Q6 magnets (and persistent current effects will therefore be smaller). However, the β-functions at the Q5 magnets reach values of more than 500 m at the end of the squeeze and powering errors due to persistent current and hysteresis effects can still play a significant role in these magnets. Fig. 11 to 16 show furthermore that a change in the slope of the gradient transition can not be avoided for all quadrupole circuits. For example, the Q4 quadrupole circuit of Beam1 (see Fig. 11) and the trim quadruple circuits for Beam2 (see Fig. 16) change the slope of the gradient transition during the squeeze.

Fig. 17 and 18 show the injection optics for Beam1 and Beam2 in IR8 and Fig. 19 and 20 the collision optics with $\beta^* = 1$ m. Fig. 21 and 22 show the corresponding crossing angle orbit bumps for Beam1 with the injection and collision optics respectively. The injection optics requirements in IR2 and IR8 differ from those in IR1 and IR5 because of the additional constraints imposed by the injection systems. An efficient protection of the cold machine against injection kicker failure scenarios requires a 90° phase advance in the vertical plane between the injection kicker MKI and the TDI protection device. This requirement can only be satisfied with $\beta^* \leq 10$ m and triplet gradients of $225/15.55\ T/m$ [3][4].

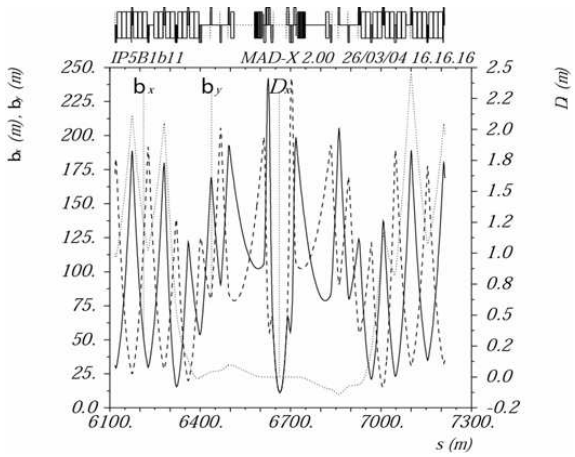

Figure 5: The transition optics with $\beta^* = 11$ m in IR5 for Beam1.

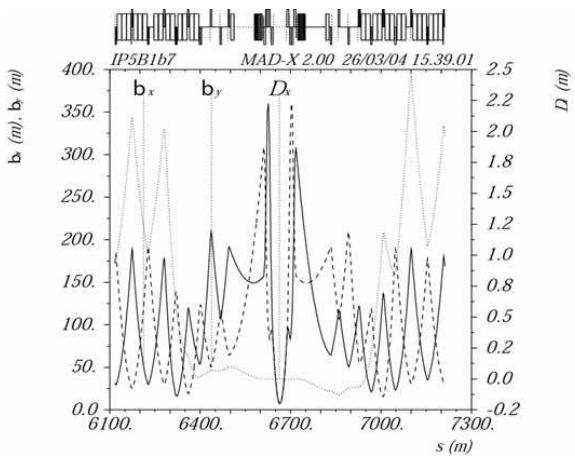

Figure 6: The transition optics with $\beta^* = 7$ m in IR5 for Beam1.

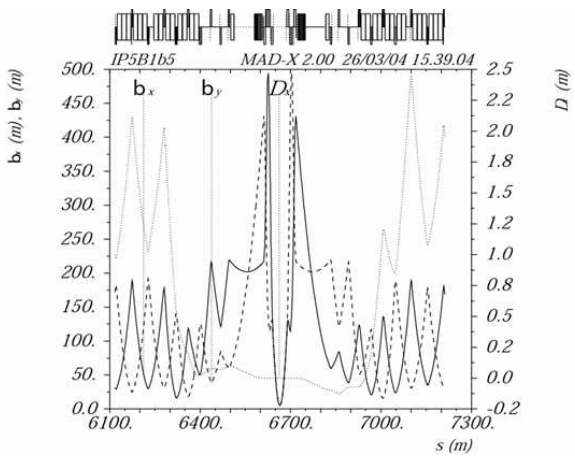

Figure 7: The transition optics with $\beta^* = 5$ m in IR5 for Beam1.

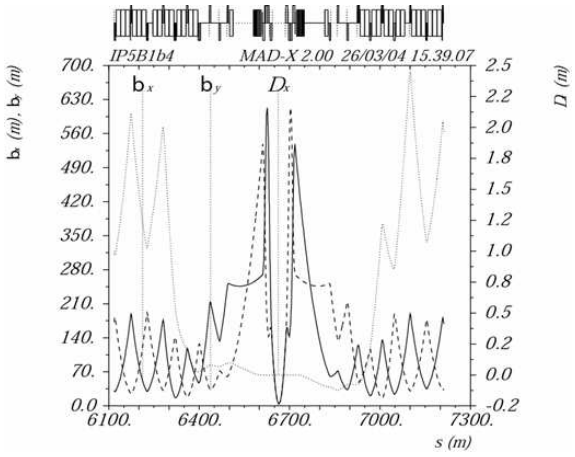

Figure 8: The transition optics with $\beta^* = 4$ m in IR5 for Beam1.

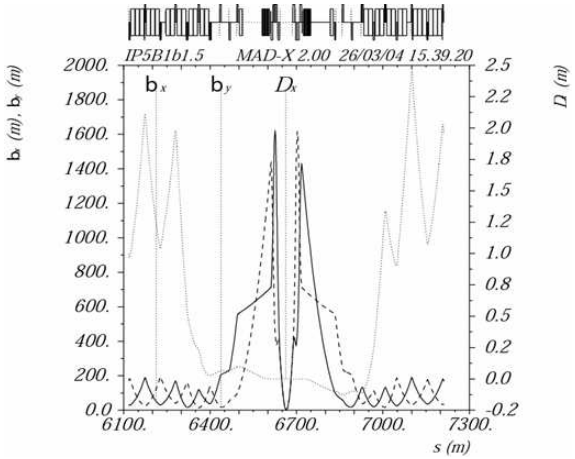

Figure 9: The transition optics with $\beta^* = 1.5$ m in IR5 for Beam1.

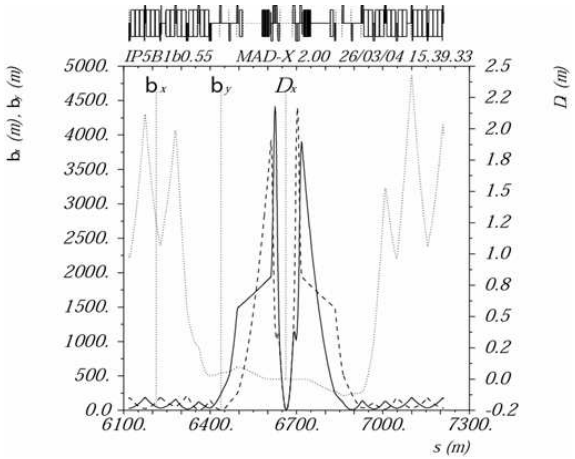

Figure 10: The transition optics with $\beta^* = 0.55$ m in IR5 for Beam1.

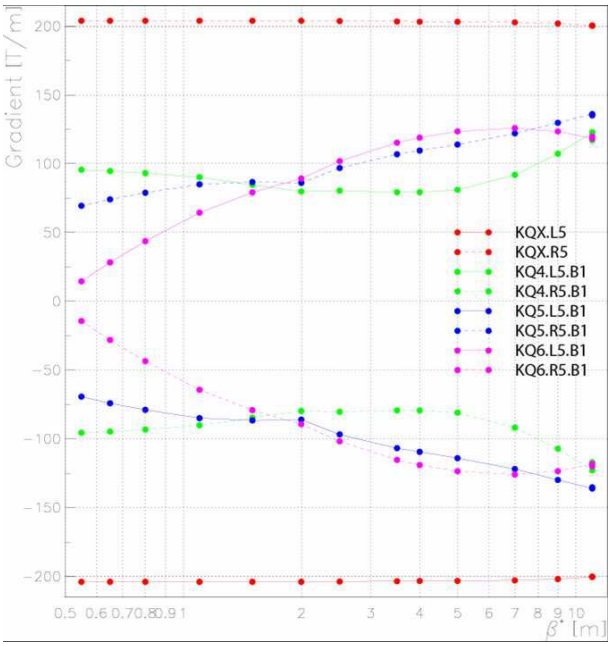

Figure 11: The normalized quadrupole gradients of the matching section for Beam1 during the squeeze.

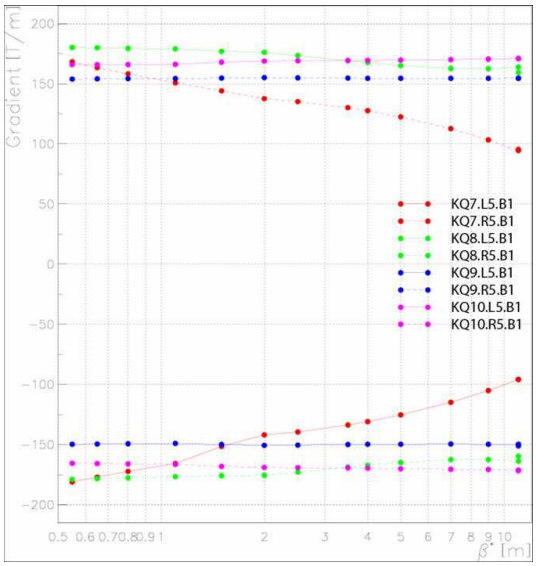

Figure 13: The normalized quadrupole gradients of the main dispersion suppressor quadrupole magnets for Beam1 during the squeeze.

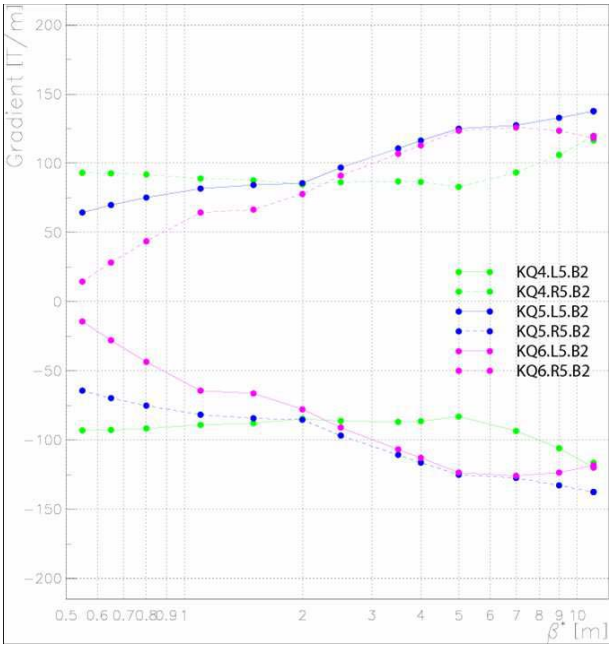

Figure 12: The normalized quadrupole gradients of the matching section for Beam2 during the squeeze.

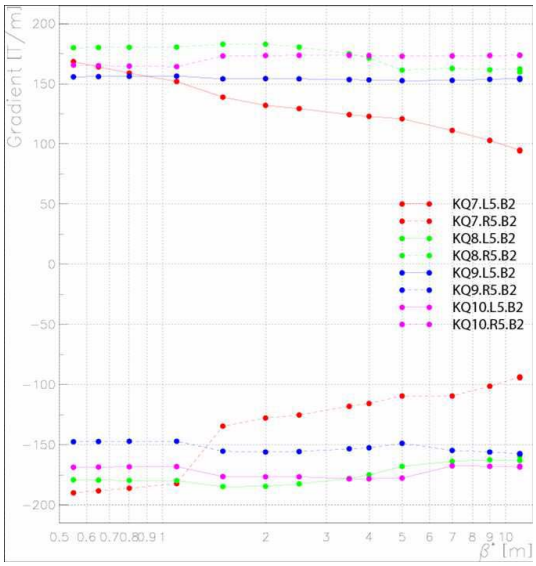

Figure 14: The normalized quadrupole gradients of the main dispersion suppressor quadrupole magnets for Beam2 during the squeeze.

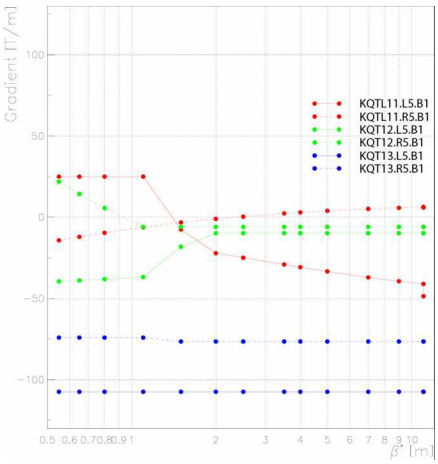

Figure 15: The normalized quadrupole gradients of the trim dispersion suppressor quadrupole magnets for Beam1 during the squeeze.

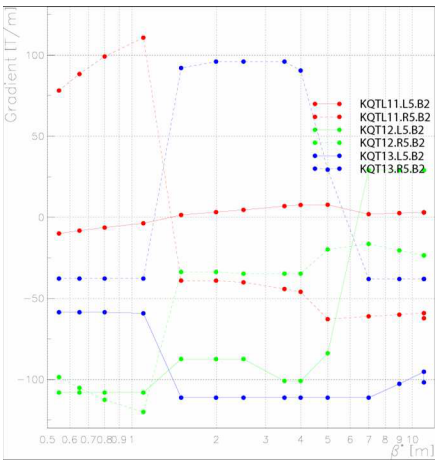

Figure 16: The normalized quadrupole gradients of the trim dispersion suppressor quadrupole magnets for Beam2 during the squeeze.

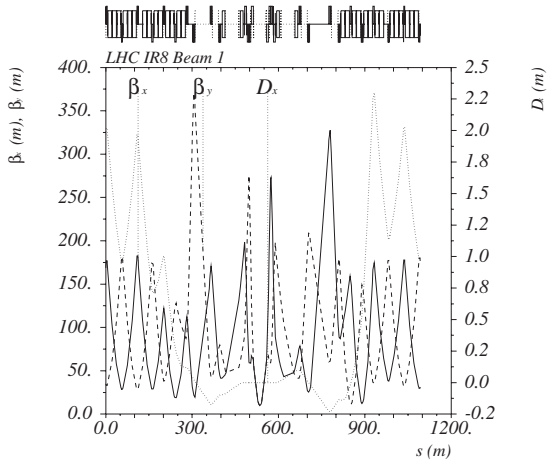

Figure 17: The injection optics for Beam1 (non-injected beam) in IR8 with $\beta^* = 10$ m.

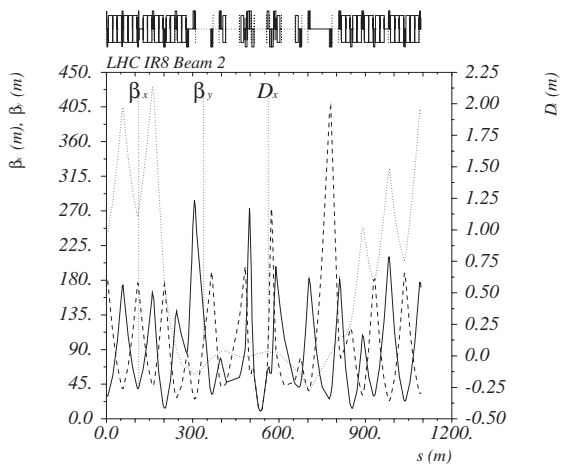

Figure 18: The injection optics for Beam2 (injected beam) in IR8 with $\beta^* = 10$ m.

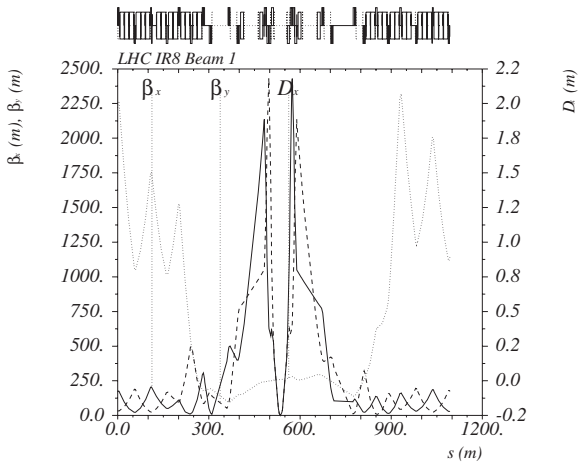

Figure 19: The collision optics for Beam1 in IR8 with $\beta^* = 1$ m.

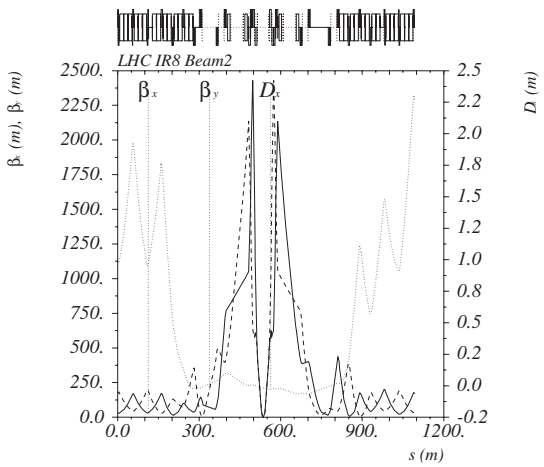

Figure 20: The collision optics for Beam2 in IR8 with $\beta^* = 1$ m.

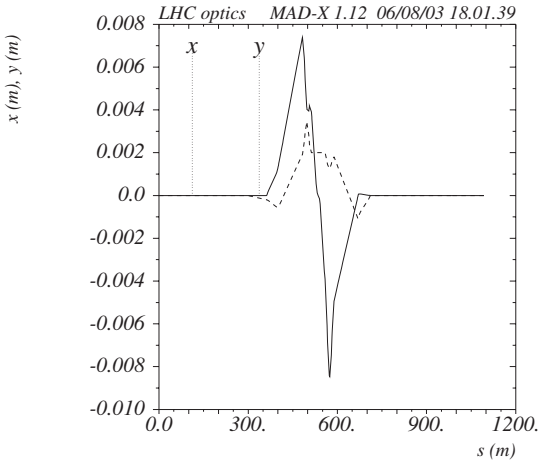

Figure 21: The crossing angle separation bump for Beam1 in IR8 for the injection optics with $\beta^* = 10$ m.

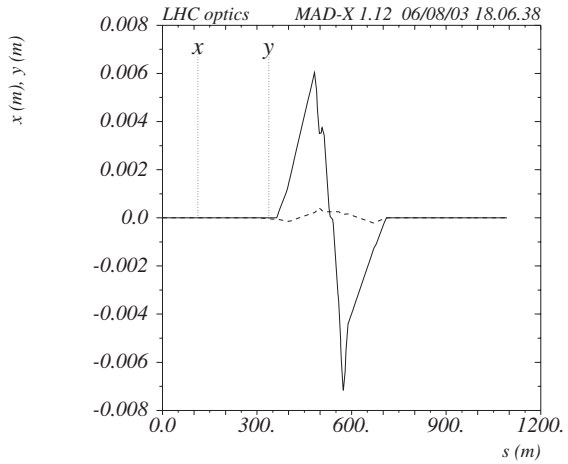

Figure 22: The crossing angle separation bump for Beam1 in IR8 for the collision optics with $\beta^* = 1$ m.

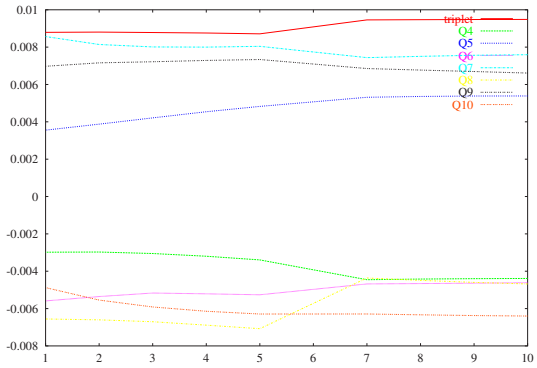

Figure 23: The normalized quadrupole gradients of the matching section on the left side in IR8 for Beam1 during the squeeze as a function of β^*.

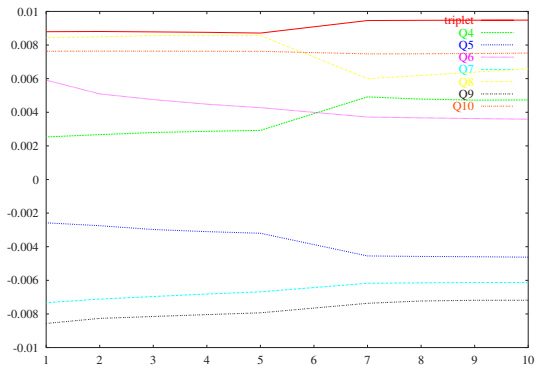

Figure 24: The normalized quadrupole gradients of the matching section on the right side of IR8 for Beam1 during the squeeze as a function of β^*.

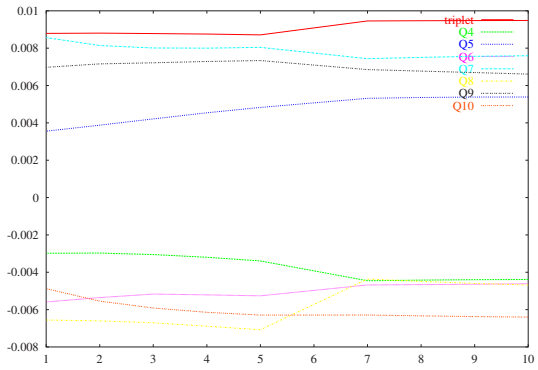

Figure 25: The normalized quadrupole gradients of the matching section on the left side in IR8 for Beam2 during the squeeze as a function of β^*.

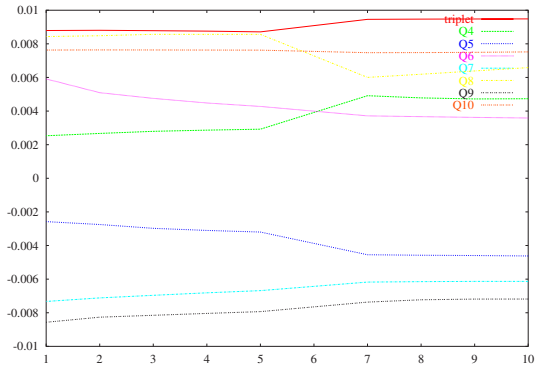

Figure 26: The normalized quadrupole gradients of the matching section on the right side in IR8 for Beam2 during the squeeze as a function of β^*.

The small β^* values imply smaller tolerances for the beam separation compared to the IR1 and IR5 configurations and the large triplet gradients imply larger than nominal gradients at top energy if the injection optics is not changed during the ramp. Fig. 23 to 26 show the gradient transitions for the individually powered insertion quadrupole magnets in IR8.

EFFECT OF GRADIENT ERRORS

β-BEAT

An error of a single quadrupole gradient causes a perturbation of the β-function along the storage ring which is given by [5]

$$\frac{\Delta\beta}{\beta_0} = \frac{-\beta_i}{2\sin 2\pi Q} \cdot l\Delta k_i \cdot \cos\left(2|\Delta\phi_i| - 2\pi Q\right), \qquad (1)$$

where β_i is the β-function at the location of the perturbed quadrupole magnet, $\Delta\phi_i$ the phase advance between location oof the perturbation and the observation point and $l\Delta k_i$ the integrated strength of the quadrupole perturbation. The perturbation due to quadrupole gradient errors is proportional to the β-function value at the perturbed quadrupole magnet. Table 4 shows the maximum β-function and gradient values for some insertion quadrupole magnets at the end of the squeeze. The first column in Table 5 shows the resulting maximum β-beat for a quadrupole error of 10 units ($\Delta k = 10 \cdot 10^{-4} \cdot k_0$). The Q1 and Q3 magnets are of the same magnet type (KEK) and are powered in series for each triplet assembly (same nominal gradient). Any β-beat due to a systematic transfer function error in the Q1 and Q3 magnets therefore adds up. The Q2 magnets of the triplet assembly are of a different magnet type (FNAL) and are powered by the same 8 kA power converter that feeds the Q1 and Q3 magnets plus an additional 6 kA 'trim' power converter. Even though the Q2 magnets have an opposite gradient sign compared to the Q1 and Q2 magnets the β-beat due to transfer function errors in the Q2 magnets therefore does not necessarily compensate the β-beat generated by the Q1 and Q3 magnets. The second column in Table 5 shows the expected β-beat for a 10 unit transfer function error in one triplet or one insertion quadrupole magnet.

The triplet magnets left and right from one IP have an opposite polarity and are spaced by a phase advance of 180° for the low-β collision optics. Assuming equal relative gradient errors inside the quadrupole magnets on both sides of the IP therefore implies a partial compensation of the β-beat. However, because the β-functions are not equal on both sides of the IP (due to the asymmetric optics) this compensation is not perfect. For $\beta^* = 0.55$ m the difference in the β-function left and right from the IP is of the order of 500 m inside the Q2 and Q3 magnets (see Fig. 4). Table 5 shows the expected total β-beat for a 10 unit transfer function error in the Q2 magnets on both sides of the IP.

Table 4: The average β-function values, quadrupole gradients, magnet lengths and beam offsets due to the crossing angle bumps for some of the insertion quadrupole magnets.

Quad. name	β_{max} **[m]**	**normalized strength** $[m^{-2}]$	**length [m]**	Δz **[mm]**
Q1	1500	0.0085	6.37	7
Q2	4000	0.0085	$2 \cdot 5.5$	7
Q3	4000	0.0085	6.37	7
Q4	1500	0.0050	3.4	2
Q7	200	0.0085	$2 \cdot 3.4$	0.5

The total β-beat budget for the machine operation in Table 3 corresponds to a gradient perturbation of either:

- 10 units transfer function error in one Q2 unit in one triplet assembly
- 15 units transfer function error in one Q1-Q3 unit in one triplet assembly (sum of Q1 and Q3 contribution)
- 35 units transfer function error in all insertion quadrupole magnets except the triplet magnets (3 σ of the incoherent sum of all contributions)
- 80 units systematic transfer function error in the Q2 units in one IP (sum weighted by the difference in the β-functions left and right from the IP)

All the above cases do not provide a large margin for transfer function errors during the end of the squeeze and the above results highlight the importance of precise transfer function measurements for all insertion quadrupole magnets. Fig. 27 and 28 show, for example, the horizontal and vertical β-beat along the LHC for a 10 unit systematic transfer function error in all triplet magnets on the left side of IP5.

The dispersion in a storage ring is given by [5]

$$D(s) = \frac{\beta(s)}{2\sin\pi Q} \cdot \oint \frac{\beta(t)}{\rho(t)} \cos\left(|\Delta\phi(t)| - \pi Q\right) dt \qquad (2)$$

where $\rho(t)$ is the radius of curvature of the main dipole magnets. A perturbation of the β-function along the storage ring therefore also changes the dispersion function in the machine. Fig. 29 shows, for example, the resulting dispersion function error along the storage ring for a systematic 10 unit transfer function error in the triplet assembly on the left side of IR5. The peak normalized dispersion error corresponds to approximately 3 % of the nominal normalized dispersion in the arc and is clearly within the tolerances given in Table 3.

Tune Error

An error of a single quadrupole gradient causes a perturbation of the total machine tune Q [5]:

$$\Delta Q = \frac{\beta_i}{4\pi} \cdot l\Delta k_i, \qquad (3)$$

Table 5: The maximum β-beat, tune and closed orbit errors in the LHC for a gradient perturbation of 10 units ($\Delta k = 10 \cdot 10^{-4} \cdot k_0$, where k_0 is the unperturbed normalized quadrupole strength) in one of the insertion quadrupole magnets. All perturbations are evaluated for the nominal tune during physics operation: $Q_x = 64.31; Q_y = 59.32$.

Quadrupole name	β**-beat [%]**	ΔQ	ΔCO [σ]
Q1	4	0.0065	0.5
Q2	20	0.03	1
Q3	10	0.017	0.8
Q2 left & right	2.5	0.004	0.3
Q4	1	0.002	0.3
Q7	0.5	0.001	0.01

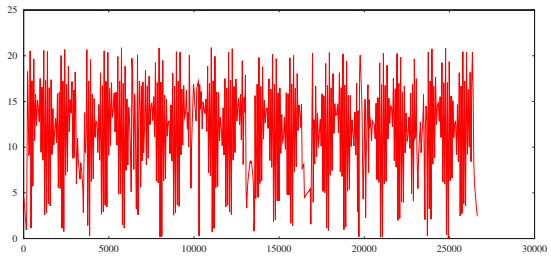

Figure 27: The horizontal β-beat in % along the LHC for a systematic 10 units transfer function error in the triplet assembly left from IP5 for the collision optics with $\beta^* = 0.55$ m.

where β_i is the β-function at the location of the perturbed quadrupole magnet and $l\Delta k_i$ the integrated strength of the quadrupole perturbation. The perturbation due to quadrupole gradient errors is proportional to the β-function value at the perturbed quadrupole magnet. The third column in Table 5 shows the expected tune shift for a 10 unit transfer function error in one triplet or one insertion quadrupole magnet. The contributions for all magnets are

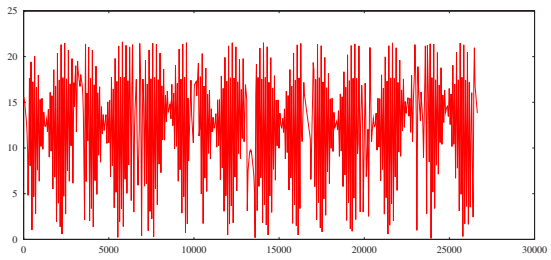

Figure 28: The vertical β-beat in % along the LHC for a systematic 10 units transfer function error in the triplet assembly left from IP5 for the collision optics with $\beta^* = 0.55$ m.

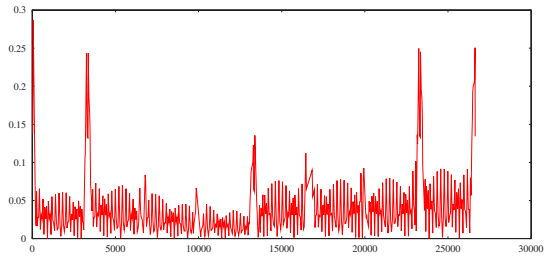

Figure 29: Change in the horizontal dispersion function in m along the LHC for a systematic 10 unit transfer function error in the triplet assembly left from IP5 for the collision optics with $\beta^* = 0.55$ m.

very close the tolerance given in Table 3. Systematic transfer function errors inside the triplet quadrupole magnets will again partially cancel because of the alternating magnet polarity of the insertion quadrupole magnets. However, due to the variation in the β-functions this cancellation can never be perfect. Assuming, for example, a systematic transfer function error of 10 units in all quadrupole magnets of one triplet assembly one still obtains a total tune shift of $\Delta Q = 0.026$ (using MAD) and the data in Table 5 underlines the necessity of a tune feedback system during the squeeze.

Closed Orbit Error

The crossing angle closed orbit bump is partially generated by a beam offset inside the triplet quadrupole magnets. An error of a single quadrupole gradient with beam offset causes a perturbation of the closed orbit along the storage ring which is given by

$$\Delta CO = \frac{\sqrt{\beta_i/\epsilon_n}}{2\sin\pi Q} \cdot l\Delta k_i \cdot \Delta z \cdot \cos\left(|\Delta\phi_i| - \pi Q\right), \quad (4)$$

where Δz is the beam offset inside the quadrupole magnet. The gradient and the crossing angle orbit bump change sign left and right from the IP. Assuming equal relative gradient errors inside the quadrupole magnets on both sides of the IP therefore implies the same deflection on both sides of the IP. The triplet magnets left and right from one IP are spaced by a phase advance of 180° for the low-β collision optics. Assuming equal relative gradient errors inside the quadrupole magnets on both sides of the IP therefore implies a closure of the orbit perturbation. However, because the β-functions are not equal on both sides of the IP (due to the asymmetric optics) this compensation is not perfect. For $\beta^* = 0.55$ m the difference in the β-function left and right from the IP is of the order of 500 m inside the Q2 and Q3 magnets (see Fig. 4). Table 5 shows the expected total closed orbit error for a 10 unit transfer function error in the Q2 magnets on both sides of the IP. Comparing the data in Table 5 with the tolerances in Table 3 illustrates that a closed orbit feedback during the squeeze is highly desirable. Fig. 30 shows, for example, the horizontal closed

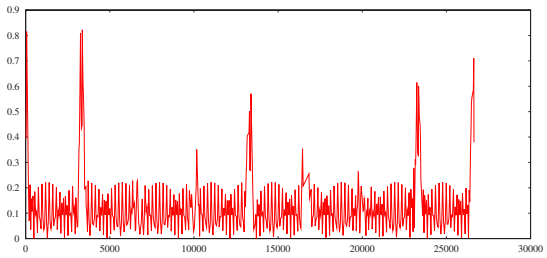

Figure 30: Change in the horizontal closed orbit [mm] along the LHC for a systematic 10 unit transfer function error in the triplet assembly left from IP5 for the collision optics with $\beta^* = 0.55$ m.

orbit error in mm along the LHC for a 10 unit systematic transfer function error in all triplet magnets on the left side of IR5.

In Chamonix 2003 it was underlined that transfer function errors of the D1 and D2 separation-recombination dipole magnets can have a significant effect on the closed orbit (10 units transfer function error in the D1 dipole magnet change the closed orbit by 3 σ in the triplet quadrupole magnets for the squeezed optics). These perturbations are proportional to the square root of the local β-function at the D1 magnet and therefore, become more important towards the end of the squeeze. Keeping the perturbations within the acceptable tolerances requires a local correction of these effects and a careful analysis to what degree the perturbations are generated by D1-D2 transfer function errors or by triplet alignment errors or by gradient error of the triplet magnets with crossing angle bump offsets.

REQUIRED ACTIONS FOR THE SQUEEZE GENERATION

The optics squeeze changes the β-functions inside the triplet quadrupole magnets and, thus, also the rms beam size in the triplet magnets and the off-momentum β-beat along the machine. The change of the rms beam size in the triplet magnets implies a re-adjustment of the collimator jaws and the change of the off-momentum β-beat a re-adjustment of the lattice sextupole circuits. The optics squeeze therefore requires, in addition to functions for the insertion region quadrupole magnet powering, functions for the collimator jaw adjustments and the lattice sextupole powering changes during the squeeze. Furthermore, the above discussions on the β-beat, tune and closed orbit perturbations due to gradient errors during the squeeze illustrate the need for online monitoring of key parameters such as closed orbit, tune and the rms beam size and, if possible, online adjustments via feedback loops.

It is not yet clear how the collimator jaws will be readjusted during the squeeze and if this readjustment can be done 'on the fly' during the squeeze or if the re-adjustment of the jaws requires a stop of the squeeze at intermediate steps.

TIME ESTIMATE FOR THE SQUEEZE

The maximum ramp rate for the trim quadrupole circuits is 10 A/s and the circuits require a maximum time of 2 minutes for changing the magnet powering over the whole accessible range. The main single quadrant circuits for the individually powered insertion quadrupole magnets also have a maximum ramp rate of 10 A/s. However, for small magnet currents (around 500 A) the maximum ramp rate reduces to only 5 A/s [6].

Figures 11 to 16 show that the maximum change of the insertion quadrupole powering in IR5 occurs for Q6. The gradient of Q6 reduces from 75 % of the nominal value for $\beta^* = 18$ m to approximately 30 % of the nominal value for $\beta^* = 1$ m and only 5 % of the nominal value for $\beta^* = 0.55$ m. The Q6 magnet is a 4 K circuit with a nominal powering of 3.6 kA. Assuming a maximum ramp rate of 10 A/s for a powering down to 30 % of the nominal gradient (ca. 1000 A) one obtains a minimum time of 4 minutes for the squeeze from $\beta^* = 18$ m to $\beta^* = 1$ m. Assuming a maximum ramp rate of 5 A/s for the powering below 30 % of the nominal gradient one obtains a minimum time of 3.5 minutes for the squeeze from $\beta^* = 1$ m to $\beta^* = 0.55$ m. Q7 is another circuit featuring a large variation of the gradient during the squeeze. Q7 is a 1.8 K circuit with a nominal powering of 5.4 kA. The gradient of the Q7 circuits increases from 50 % of the nominal value for $\beta^* = 18$ m to almost 100 % of the nominal value for $\beta^* = 1$ m. Assuming a maximum ramp rate of 10 A/s one obtains a minimum time of 5 minutes for the squeeze from $\beta^* = 18$ m to $\beta^* = 1$ m which is slightly larger than the length imposed by the Q6 circuit.

Combining the limitations imposed by the Q6 and Q7 circuits one obtains a minimum time of 5 minutes for the squeeze from $\beta^* = 18$ m to $\beta^* = 1$ m and a minimum time of 8.5 minutes for the squeeze from $\beta^* = 18$ m to $\beta^* = 0.55$ m. In case the squeeze can not be done in one go and requires intermediate stops, either for correction circuit or collimator jaw adjustments, one needs to add additional time for the round-off and re-start of the current ramp at each intermediate step. The total time for the squeeze can be significantly larger than the above estimates in this case.

SUMMARY AND COMMENTS

The above analysis shows that an operation of the LHC within the tight tolerances requires an accurate knowledge of the insertion quadrupole transfer functions. It should be underlined here that, unlike the arc quadrupole magnets, the insertion quadrupole magnets do not all follow the same powering cycle during the ramp and squeeze. This variation of the magnet powering for otherwise identical magnets has to be kept in mind for the measurement of the magnet transfer functions during dedicated magnet tests.

One option for reducing the optics perturbation during the squeeze is to squeeze only one IR at the time. However, the disadvantage of this approach is that it further increases the minimum time for the squeeze and that it requires a

larger number of readjustments in the lattice corrector circuits and collimator jaws.

A potential strategy for setting up the squeeze is to first squeeze one IR at the time without crossing angle. This provides additional margins for the triplet magnet aperture and, thus, requires less accurate adjustments of the collimator jaws or larger tolerances in the optics perturbations. This stage of the squeeze setup can be used for disentangling the D1 transfer function and triplet alignment errors, establishing matched intermediate solutions (minimize the β-beat during the squeeze) and implementing collimator adjustments for the intermediate stops. As a next step one could squeeze one IR at a time with crossing angle. This stage of the squeeze setup can be used for correcting the closed orbit errors at each intermediate step and implementing the non-linear triplet corrector settings. Next one could aim at minimizing the number of intermediate stops during the squeeze and to implement online feedback loops. The number of required intermediate stops during the squeeze could potentially be reduced by implementing a partial squeeze already during the ramp. As a final step one could establish a parallel squeeze in all IRs in order to minimize the required total time for the squeeze in all IRs.

During the workshop it was not yet clear what is the reproducibility of the magnet transfer functions for a circuit that operates sonly at 5 % of its nominal powering level (what is the contribution of persistent current effects and what is the dynamic behavior?). It was also not clear at the time of the workshop how many intermediate stops are necessary for a squeeze (we need a procedure for the squeeze and collimator setup) and what is the change in the magnet transfer function knowledge if the squeeze is stopped and restarted (what is the relevance of beam based measurements at the intermediate steps for a squeeze without stops?). All the above points need to be addressed before the machine startup and before the magnetic magnet measurement program stops in SM18.

REFERENCES

[1] LHC Design report Volume I, CERN-2004-003; 4. June 2004.

[2] Stephane Fartoukh at the 23. LTC meeting, 31. March 2004, http://lhcp.web.cern.ch/lhcp/ab-ltc/ltc_2004-05.html

[3] 'Optics Solutions in IR2 for Ring1 and Ring2 of the LHC Version 6.0', O. Brüning, LHC Project Note 188, April 1998

[4] 'Optics Solutions in IR8 for Ring1 and Ring2 of the LHC Version 6.0', O. Brüning, LHC Project Note 193, June 1998

[5] 'Basic Course on Accelerator Optics', J. Roßbach and P. Schmüser, DESY M-93-02, February 1993

[6] F. Bordry at the 33. LTC meeting, 27. October 2004, http://lhcp.web.cern.ch/lhcp/ab-ltc/ltc_2004-15.html